

Original Research

Targeted Knockdown of Hepatic Δ -5 Fatty Acid Desaturase FADS1 Aggravates Atherosclerosis in ApoE^{-/-} Mice

Qiulei Liu¹, Peng Wang¹, Zhao Yang², Yue Dai², Sheng Wang^{1,*}¹Department of Vascular Surgery, Beijing Anzhen Hospital, Capital Medical University, 100029 Beijing, China²Department of Cardiac Surgery, Beijing Anzhen Hospital, Capital Medical University, 100029 Beijing, China*Correspondence: sdws188@163.com (Sheng Wang)

Academic Editor: Raffaele Serra

Submitted: 24 September 2023 Revised: 15 February 2024 Accepted: 6 March 2024 Published: 29 March 2024

Abstract

Background: The endogenous metabolism of polyunsaturated fatty acids is regulated by the fatty acid desaturase (FADS) gene cluster and is strongly associated with diseases such as atherosclerosis, dyslipidemia, and type 2 diabetes. However, the association between FADS and atherosclerosis remains a subject of debate. **Methods:** In this study, we specifically investigated the physiological role of Δ -5 fatty acid desaturase (FADS1) in aortic and peripheral vessel (namely, the femoral artery) atherosclerosis by targeting the selective knockdown of hepatic *Fads1* in apolipoprotein E-null (ApoE^{-/-}) mice with antisense oligonucleotides (ASOs). **Results:** Knockdown of hepatic *Fads1* in ApoE^{-/-} mice exacerbated aortic atherosclerosis and non-alcoholic fatty liver disease (NAFLD), resulting in weight loss. Upregulation of FADS1 mRNA expression in more severe atherosclerosis vascular tissues potentially caused the upregulation of angiotensin-like 4 expression. **Conclusions:** Our study demonstrated that knockdown of hepatic *Fads1* in ApoE^{-/-} mice aggravates spontaneous atherosclerosis and NAFLD but does not affect peripheral atherosclerosis (femoral artery) induced by vascular cuff combined with tandem stenosis.

Keywords: Δ -5 fatty acid desaturase; atherosclerosis; antisense oligonucleotides; angiotensin-like 4

1. Introduction

Fatty acid desaturase (FADS) is a critical enzyme in polyunsaturated fatty acid (PUFA) metabolism, and gene polymorphisms in FADS affect the activity and function of FADS [1,2], which in turn affect metabolic activities in the body such as lipid concentrations, cardiovascular disease risk, pregnancy, cognitive function, Alzheimer's disease, overweight, and type 2 diabetes mellitus [3–5]. Genetic studies have shown that variants in *Fads1*, encoding the Δ 5 fatty acid desaturase, and *Fads2*, encoding the Δ 6 fatty acid desaturase, are most directly genetically linked to PUFA levels and that the FADS gene cluster (*Fads1-2-3*) is the most important locus for influencing PUFA metabolism [6–9]. Given that genetic studies have provided a theoretical foundation for exploring the impact of the FADS gene cluster on the pathogenesis of atherosclerotic cardiovascular disease and altered expression of FADS1 in several human genetic studies, including coronary artery disease, stroke, and aortic valve stenosis and calcification [10,11], we focused our study on the effect of FADS1 on atherosclerosis in mice.

Mice with *Fads1* knockout or knockdown exhibited different phenotypes in atherosclerosis for unclear reasons. Regardless of the type of model mice, the phenotype may be associated with the production of specialized pro-resolving mediators or pro-inflammatory mediators regulated by FADS1 [12–14]; however, it is unknown whether *Fads1* affects atherosclerosis by regulating specific signal-

ing pathways. Studies have shown that FADS1 overexpression can promote carcinogenesis and angiogenesis by activating AKT/mammalian target of rapamycin (mTOR) signaling, meanwhile activation of phosphoinositide 3-kinase/AKT/mTOR signaling can promote the occurrence and development of atherosclerosis by aggravating the inflammatory response and causing endothelial dysfunction [15]. Given the regulatory role of *Fads1* in atherosclerosis, we speculate that *Fads1* can regulate endothelial cell function through AKT/mTOR signaling and experimentally explored the downstream proteins of this axis; this protein may ultimately influence atherosclerosis.

To overcome the obstacle of *Fads1*^{-/-} leading to impaired growth and premature death in mice [13,16,17], we used triantennary N-acetyl galactosamine (Tri-GalNAc)-modified antisense oligonucleotides (ASOs) to target knockdown of *Fads1* in the mouse liver, thus avoiding the lethality caused by *Fads1* deletion. The results showed that hepatic *Fads1* knockdown in apolipoprotein E-null (ApoE^{-/-}) mice exacerbated atherosclerosis, and angiotensin-like 4 (ANGPTL4) expression was upregulated in aortic tissues with more severe atherosclerosis. This study provides a new perspective to explore the effect of FADS1 on atherosclerosis.

2. Materials

Collagenase (type IV) (Cat No. C4-BIOC) used for the perfusion, Percoll (Cat No. P1644) used for the density



gradient centrifugation, and trypsin (Cat No. T4049) were purchased from Sigma-Aldrich (St. Louis, MO, USA). Dulbecco's Modified Eagle's Medium (DMEM; Cat No. 11995065), Opti-Minimal Essential Medium (Opti-MEM Cat No. 31985070), and fetal bovine serum (FBS; Cat No. A5670701) were purchased from Gibco (Waltham, MA, USA). D-Hank's (Hank's Balanced Salt Solution; Cat No. 14175103) and Lipofectamine 2000 (Cat No. 11668027) were purchased from Invitrogen (Carlsbad, CA, USA). ASOs were produced by Synbio Technologies (Suzhou, China). The NCTC-1469 adherent cell line (Cat No. SCC-220211) and Mycoplasma Detection Kit (Cat No. CA1080) were purchased from Solarbio Technology Co., Ltd. (Beijing, China). Hematoxylin and eosin (H&E) staining reagent (Cat No. G1003) and Oil Red O staining reagent (Cat No. G1015) were purchased from Servicebio (Wuhan, China). Antibodies against cluster of differentiation 31 (CD31) (Cat Nos. GB11063-1, GB12063), alpha smooth muscle actin (α -SMA; Cat No. GB111364), F4/80 (Cat No. GB11027), and vascular cell adhesion molecule 1 (VCAM-1; Cat No. GB113498) were purchased from Servicebio. Antibody against ANGPTL4 (Cat No. 18374-1-AP) was purchased from the Proteintech Group (Wuhan, China). Fluorescent secondary antibodies were purchased from the Proteintech Group (Cat Nos. SA00013-7, SA00013-8) and Servicebio (Cat Nos. GB25301, GB25303). Bovine serum albumin (BSA; Cat No. GC305010) was purchased from Servicebio. Wild-type mice used for obtaining primary hepatocytes and ApoE^{-/-} mice used for constructing models, both in the C57BL/6J genetic background, were purchased from HFK Bio-Technology Ltd. (Beijing, China). Other materials used in this study will be detailed accordingly in later sections.

3. Methods

3.1 Cell Culture

NCTC-1469 cells were cultured in DMEM containing 10% FBS. Subculturing was performed when the cells had grown to logarithmic phase. Primary mouse hepatocytes isolated from 8-week-old male C57BL/6J wild-type mice by collagenase perfusion (type IV) [18] were cultured in DMEM containing 10% FBS. Primary mouse hepatocytes were identified by cytokeratin-18 immunofluorescence, and the purity could be more than 90%. Cells were all cultured in a humidified incubator at 37 °C and 5% CO₂. The cells were tested accordingly to exclude mycoplasma contamination, and validated by short tandem repeat profiling.

3.2 Antisense Oligonucleotide (ASO) and Administration

Fads1-ASO (GGTGCATGTTGATATCGGGG) targeting mouse FADS1 mRNA and control-ASO (ATTC-GACGGGCTTACGTTG), which does not target any sequence in the mouse genome, were developed and synthesized by Synbio Technologies. Each ASO consisted of five

nucleotides on the 5' and 3' ends of the ASO with a 2'-O-methoxyethyl modification and a central 10-base DNA "gap", and all bases in ASO were modified by phosphorothioate. In addition, ASO for intraperitoneal (IP) injection in mice was modified with Tri-GalNAc at the 3' end. *Fads1*-ASO was confirmed to bind with 100% complementarity to mouse FADS1 mRNA and does not bind to any other mRNA with complete complementarity within the mouse transcriptome. Lyophilized *Fads1* and control ASO were diluted in TE buffer to a concentration of 1 μ g/ μ L for the cell experiment. For the animal experiment, ASO was diluted in normal saline. Basic information about ASOs is shown in Table 1.

3.3 ASOs Transfection In Vitro

3.3.1 Transfection of ASOs Using Lipofectamine 2000

(1) One day before transfection, 5–8 \times 10⁵ NCTC-1469 cells per well were cultured in a 12-well plate in 800 μ L DEME without antibiotics to attain 80–90% confluence at the time of transfection.

(2) For each transfection sample, ASO–Lipofectamine 2000 complexes were prepared as follows: 1 μ g ASO was diluted in 50 μ L Opti-MEM, and mixed gently.

(3) The stock Lipofectamine 2000 was mixed gently before use, and then 3 μ L was diluted in 50 μ L Opti-MEM. The solution was mixed gently and left to stand for 5 min at room temperature.

(4) Five minutes after dilution of Lipofectamine 2000, the diluted ASO was combined with the diluted lipid (total volume was 100 μ L). The solution was mixed gently and left to stand for 20 min at room temperature to allow the ASO–Lipofectamine 2000 lipoplexes to form.

(5) The transfection complex (100 μ L) was added to each well, followed by gentle mixing by rocking the plate back and forth.

(6) The cells were incubated at 37 °C in a humidified incubator with 5% CO₂ for 24 h until they were ready to assay for gene knockdown using RT-PCR.

3.3.2 Use of ASO-Tri-GalNAc to Transfect Primary Mouse Hepatocytes

After verifying that ASO could effectively inhibit *Fads1* expression, ASO was modified by Tri-GalNAc (i.e., antisense-3) (Table 1), and its transfection efficiency was verified *in vitro*. The isolated primary hepatocytes from 8-week-old male wild-type mice in the C57BL/6J genetic background were plated in a 12-well plate at 80–90% density, followed by the addition of 0.8 mL Dulbecco's Modified Eagle Medium (DMEM) (without antibiotics). Cells were cultured in an incubator with 5% CO₂ at 37 °C overnight. ASO-Tri-GalNAc transfection was performed the next day. Before transfection, the ASO-Tri-GalNAc dry powder was diluted in 1 μ g/ μ L working solution in phosphate-buffered saline (PBS). For each transfection sample, the concentration of ASO-Tri-GalNAc was 3

Table 1. Chemical composition and analytical data for ASOs.

ASO	Target	Sequence	Calcd. Mass
Antisense-1	Mouse <i>Fads1</i>	FITC-GGTGCATGTTGATATCGGGG	7580.0
Antisense-2	Mouse <i>Fads1</i>	FITC-GGTGCATGTTGATATCGGGG-GalNAc	9691.6
Antisense-3	Mouse <i>Fads1</i>	GGTGCATGTTGATATCGGGG-GalNAc	9154.0
Control	Mouse None	FITC-ATTCGACGGGCTTTACGTTG	7444.6

Note: FITC probe modification of the 5' end of ASO; blue bases represent five nucleotides on the 5' and 3' ends of the ASO with a 2'-O-methoxyethyl modification; GalNAc represents Tri-GalNAc modification of the 3' end of the ASO. ASOs, antisense oligonucleotides.

µg per well; the control group only had PBS. The cells were incubated at 5% CO₂, 37 °C for 24 h until they were ready to assay for transfection efficiency. Transfection efficiency was analyzed using flow cytometry with the excitation setting at 488 nm. At least 5000 cells were acquired, and Cell Quest software was used to analyze the data.

3.4 In Vivo Assays

To verify the effectiveness of ASO-Tri-GalNAc (i.e., antisense-3), ApoE^{-/-} male mice in the C57BL/6J genetic background were selected for intraperitoneal injection (IP) injection twice a week, whereas the control group was only injected with normal saline. One week later, RNA from the mouse liver was extracted, and reverse transcription-polymerase chain reaction (RT-PCR) was performed to verify the inhibitory effect of ASO-Tri-GalNAc on *Fads1* (Fig. 1D,E).

3.5 Animal Treatment

3.5.1 Mice Care and Grouping

This study was conducted following the regulations of the Animal Ethics Committee of Beijing Anzhen Hospital (2022174X; Beijing, China). Wild-type and ApoE^{-/-} mice, both in the C57BL/6J genetic background, were purchased from HFK Bio-Technology Ltd. Mice were all maintained at 25 ± 1 °C in a specific-pathogen free environment with a 12 h light/dark cycle. All mice were fed a high-lipid diet (20% fat, 1.25% cholesterol, and 0.5% sodium cholate; Jiangsu Medicine Ltd., Jiangsu Province, China). ApoE^{-/-} mice were divided into the Normal Group (n = 8), Normal Saline Group (n = 8), and ASO Group (n = 8) using the random number method.

3.5.2 Mouse Models and Surgery Protocol

ApoE^{-/-} mice in the Normal Saline Group and ASO Group underwent IP injection with normal saline (200 µL) or ASO-Tri-GalNAc (15 nmol antisense-3 dissolved in 200 µL normal saline) twice a week. ApoE^{-/-} mice in the Normal Group did not undergo IP injection. We performed surgical interventions in mice to investigate the effect of hepatic *Fads1* knockdown on peripheral arteries. At 12 weeks of age (after being fed a high-lipid diet for 4 weeks), three groups were anesthetized by ketamine (100 mg/kg) and xylazine (10 mg/kg) mixture through IP injection. Then mice

received polythene cuff (0.6 mm inner diameter, 1.0 mm outer diameter, and 3 mm in length; Shandong Academy of Pharmaceutical Sciences, Jinan, China) placement and tandem stenosis around the right common femoral artery [19,20]. After anesthesia, mice were on a heating pad at 37 °C, and the shallow blood flow in the legs of mice was measured by a laser Doppler blood perfusion detector (PF5000; Perimed Instruments, Stockholm, Sweden) before the surgery. Then a longitudinal incision was made approximately 1.0 cm from the right inguinal ligament to the knee joint. The neurovascular sheath was carefully separated, and the arteries, veins, femoral nerve, and branches were dissociated. A model of femoral artery atherosclerosis was constructed with the distal point of ligation 1 mm from the right common femoral artery bifurcation and the proximal point of ligation 2 mm from the distal stenosis. First, femoral artery stenosis was induced by ligation of 8-0 non-absorbent sutures around the femoral artery, mediated by a 100 µm needle, and the needle was removed after ligation. Second, the polythene cuff was loosely wrapped around the right common femoral artery to prevent damage to veins and nerves during surgery. After surgery, a laser Doppler blood perfusion detector was used to detect the superficial blood perfusion of the legs of mice after the operation to ensure that the blood flow of the limbs on the operating side decreased by 30–50% compared with that before the operation, to control the stability of the model.

3.6 Histology and Immunofluorescence

Mice were perfused from the left ventricle with PBS and heparin (250 U/kg). The aorta and three branches of the arch of mice were separated and fixed in 4% paraformaldehyde solution for subsequent Oil Red O staining. After complete dissection of bilateral femoral arteries, they were placed in optimal cutting temperature compound, rapidly frozen in liquid nitrogen, and stored at –20 °C for subsequent H&E, Oil Red O, and immunostaining. Part of the liver tissue was taken and treated similarly for subsequent Oil Red O staining [21,22].

The fat on the periphery of the aorta was removed, and the blood vessel was carefully dissected longitudinally along the vessel wall with scissors, followed by staining in Oil Red O solution, differentiation in 60% isopropanol, and washing with distilled water to terminate the differen-

tiation. Finally, photos were taken (D70; Canon, Tokyo, Japan). Multiple sections (7 μm) were prepared and stained for morphological observation with H&E, Oil Red O, and immunofluorescence. H&E and Oil Red O staining were conducted according to the instructions for the experimental reagents. For immunocytochemistry staining, sections were sealed by incubation in 3% BSA for 90 min at room temperature and then incubated with primary antibody at 4 $^{\circ}\text{C}$ overnight. Then the sections were rewashed five times with PBS (30 s each), followed by incubation with fluorescently labeled secondary antibodies for 30 min at room temperature. After washing three times with PBS (30 s each), samples were visualized with the Nikon Eclipse 80i upright microscope (Nikon, Tokyo, Japan). Quantitative analysis of histological staining and fluorescence was conducted using ImageJ software [23].

3.7 Body Weight Measurement and Glucose Tolerance Testing

Each mouse was weighed weekly at a fixed time starting from 8 weeks old; mice were fed *ad libitum* before weighing. Glucose tolerance tests were performed after a 16 h fast by injecting 1 g/kg body weight glucose into the peritoneal cavity. Tail vein blood glucose levels were measured using a commercial glucometer (One Touch; Johnson & Johnson, New Brunswick, NJ, USA). Glucose tolerance tests were performed on three groups of mice at 20 weeks old.

3.8 Plasma Lipid and Inflammatory Cytokines Analyses

At the end of the experiment, the carotid artery was severed to collect blood from mice. The blood was collected with a 1 mL syringe moistened with heparin beforehand. The blood was centrifuged at 10,000 g for 10 min at 4 $^{\circ}\text{C}$ to remove any remaining insoluble material and then the plasma samples were stored at -80°C . The contents of triacylglycerol, total cholesterol, high-density lipoprotein cholesterol (HDL-C), and low-density lipoprotein cholesterol (LDL-C) in the plasma of mice were detected with an automatic biochemical analyzer (Chemray 800; Rayto Life and Analytical Sciences, Shenzhen, China) with the test kits (Cat Nos. K068b, K074a, K075, K076; Changchun Huili Biotech Ltd., Changchun, China). The enzyme-linked immunosorbent assay (ELISA) was used to detect the inflammatory cytokines using the enzyme label detector (BioTeK, Epoch, Winooski, VT, USA) with the test kits (Cat Nos. 88-7324 and 88-7013; Thermo Fisher Scientific, Waltham, MA, USA; Cat Nos. 202/2-48, 204/2-48; Multisciences, Hangzhou, China).

3.9 RNA Isolation and Quantitative RT-PCR

RNA was isolated from cells and tissues using the Quick-RNA Purification Kit (Cat No. RN001; ESscience Biotech, Beijing, China) according to the manufacturer's instructions. For mRNA expression analysis, 2 μg total

RNA was reverse transcribed using the GoScriptTM Reverse Transcription System (Cat No. A5001; Promega, Beijing, China). Quantitative PCR (qPCR) was performed using the BlazeTaqTM Probe qPCR Mix (GeneCopoeia, Rockville, MD, USA) on the CFX Connect Real-Time PCR Detection System (Bio-Rad, Hercules, CA, USA). The expression values were normalized to the housekeeping genes β -actin or GAPDH mRNA expression levels and were calculated based on the $2^{-\Delta\Delta\text{CT}}$ method.

3.10 Western Blotting

Samples were homogenized in ice-cold lysis buffer consisting of 50 mM Tris-HCl (pH 7.4), 150 mM NaCl, 1 mM EDTA-2Na, 1% Triton X-100, 1% sodium deoxycholate, and 0.1% sodium dodecyl sulfate (SDS). A total of 30 μg protein per sample was resolved by SDS-polyacrylamide gel electrophoresis (5%), electrotferred to polyvinylidene fluoride membrane, and imaged using the ChemiScope 6100 Imaging System (Clinx Science Instruments Co. Ltd., Shanghai, China). Primary antibodies for Western blotting were ANGPTL4 (Cat No. 18374-1-AP; Proteintech), GAPDH (Cat No. GB15004; Servicebio) raised in rabbit, and Prestained Protein Marker (Cat No. G2083; Servicebio) as internal standards. The secondary antibody for Western blotting was anti-rabbit conjugated to horseradish peroxidase (Cat No. GB23303; Servicebio).

3.11 Statistical Analyses

Results are expressed as the mean \pm standard error of the mean. All data were analyzed using the *t*-test or one-way analysis of variance where appropriate, followed by Tukey's Honest Significant Difference post hoc analysis. *p*-values of <0.05 *, <0.01 **, <0.001 ***, <0.0001 **** were considered significant. SPSS 20.0 (IBM Corp., Chicago, IL, USA) and GraphPad Prism 8.3.0 software (GraphPad Software, Inc., San Diego, CA, USA) were used for statistical analyses and chart drawing.

4. Results

4.1 ASO-Tri-GalNAc Effectively Inhibits the Expression of *Fads1* in the *ApoE*^{-/-} Mouse Liver

ASO-Tri-GalNAc (i.e., antisense-3) can enter mouse hepatocytes without transfection reagents, and the transfection efficiency was about 85% (Fig. 1A–C). The expression of hepatic *Fads1* was effectively inhibited by IP injection in *ApoE*^{-/-} mice, and the inhibitory effect was enhanced by increasing the injection dose. To ensure that the drug dose did not affect the health of the *ApoE*^{-/-} mice and that the expression of *Fads1* could be effectively knocked down, we did not choose a protocol in which the higher the injected drug dose, the better. We adopted the following doses based on the experimental results (Fig. 1D,E): *ApoE*^{-/-} mice in the ASO Group were injected IP twice weekly with 15 nmol ASO-Tri-GalNAc (dissolved in 200 μL normal saline).

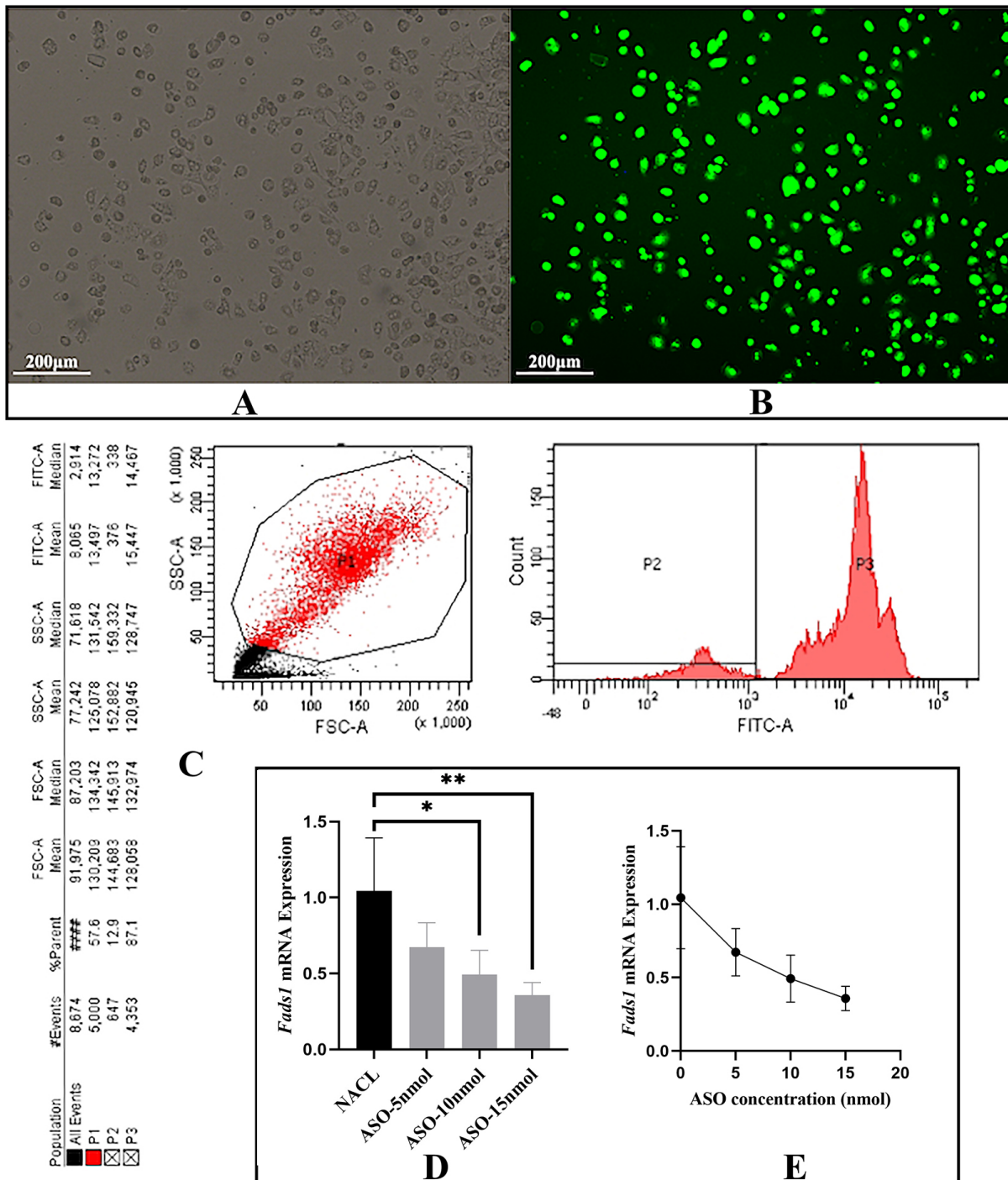


Fig. 1. *In vitro* transfection rate determination and *in vivo* validation of effectiveness of ASO-Tri-GalNAc. (A) Optical microscopic view of mouse hepatocytes. (B) Fluorescence microscopic view of ASO-Tri-GalNAc transfected into hepatocytes under the same field of view. (C) Flow cytometry to determine the number of cells transfected with ASO-Tri-GalNAc as a percentage of total cells. (D,E) ASO-Tri-GalNAc effectively inhibited *Fads1* expression in the liver of ApoE^{-/-} mice, and the inhibitory effect was enhanced with increasing injection dose (n = 4). Scale bar, 200 μ m. (*, $p < 0.05$, **, $p < 0.01$)

4.2 Successful Construction of Mouse Models

There were no deaths in the three groups of high-fat diet ApoE^{-/-} mice during the study, and all mice had surgical interventions at 12 weeks of age to establish femoral atherosclerosis. The Normal Group did not undergo IP in-

jection of any fluid. The Normal Saline Group and ASO Group were IP injected with normal saline (200 μ L) or ASO-Tri-GalNAc (15 nmol antisense-3 dissolved in 200 μ L normal saline) twice a week (Fig. 2A). We successfully constructed a model of femoral atherosclerosis by

femoral artery cuff placement combined with tandem stenosis (Fig. 2B–D). Acute ischemia symptoms of the lower limbs, such as lower limb skin temperature reduction, dull skin color, and intermittent claudication, could be observed in mice on the first day after surgery. The symptoms were reduced on the third to fifth day after surgery and completely relieved on the first week after surgery, which was considered to result from lateral branch compensation and limb adaptation. No lower limb gangrene occurred in mice during the 8-week postoperative experimental cycle, and other activities were unaffected.

4.3 Knockdown of Hepatic *Fads1* Aggravates Aortic Atherosclerosis

We found that ASO-Tri-GalNAc-mediated knockdown of liver *Fads1* significantly aggravated atherosclerosis (Fig. 3A,B). The aortic root lesion area in the ASO Group statistically differed from the Normal Group but did not statistically differ from the Normal Saline Group; the area ratio of plaque/vessel in the ASO Group statistically differed from the Normal Group and Normal Saline Group (Fig. 3C,D). We also found that ANGPTL4 expression was upregulated in the aorta of the ASO Group, whereas ANGPTL4 expression was not found in the Normal Group or Normal Saline Group (Fig. 3E,F). Interestingly, FADS1 mRNA expression in the ASO Group was upregulated in the aorta, inconsistent with the downregulation of hepatic FADS1 mRNA expression (Fig. 3G). Further analysis of the expression levels of signaling pathways in the aorta revealed the upregulation mRNA expression of mTOR complex 1 (mTORC1), AKT1, and ANGPTL4 in the ASO Group compared to the Normal Saline Group (Fig. 3H–J).

4.4 Knockdown of Hepatic *Fads1* did not Affect Modeling-Induced Atherosclerosis of the Femoral Artery

To explore the effects of hepatic *Fads1* knockdown on the peripheral arteries, by establishing a model of femoral atherosclerosis and the femoral artery between the proximal and distal ligation sites was selected for Oil Red O staining, we found that selective knockdown of liver *Fads1* had no significant effect on femoral atherosclerosis in mice (Fig. 4A). Three groups of mice both developed severe atherosclerosis in the femoral artery; however, there was no difference in the ratio of plaque area to the area under the internal elastic plate (Fig. 4B). The percentage of plaque area in the femoral artery was higher than that in the aortic root and aorta in all three groups of mice (Fig. 4C). Femoral artery immunofluorescence showed prominent infiltration of macrophages, proliferation of smooth muscle cells, incomplete arrangement of endothelial cells, and the upregulated expression of VCAM-1 in the femoral atherosclerotic sites of mice in the three groups (Fig. 4D). However, there was no difference in the area proportion of positive cells of the three groups (Fig. 4E–G).

4.5 Effects of Knockdown of Hepatic *Fads1* on Metabolism and Inflammation

We found that selective knockdown of liver *Fads1* did not affect plasma lipid and inflammatory cytokine levels (Fig. 5A–G). There was no difference in the mRNA expression of pro-inflammatory interleukin 6 (IL-6) and anti-inflammatory IL-10 in the aorta between the Normal Saline Group and ASO Group (Fig. 5H,I). Previous studies have shown that *Fads1* knockout mice generated by a gene-trapping strategy are lean relative to wild-type littermates [24]. To confirm whether selective knockdown of hepatic *Fads1* would affect body weight, we monitored the body weight of mice and found a significant reduction in body weight at 19–20 weeks of age (Fig. 5J). Moreover, there was a trend of improved glycemic control in the ASO Group mice at 20 weeks of age (Fig. 5K).

4.6 Knockdown of Hepatic *Fads1* Aggravates Non-Alcoholic Fatty Liver Disease

Liver Oil Red O staining showed that selective knockdown of liver *Fads1* significantly aggravated non-alcoholic fatty liver disease (NAFLD) (Fig. 6A). Given that ANGPTL4 was highly expressed in liver and adipose tissue, we explored whether downregulation of hepatic *Fads1* would affect ANGPTL4 production. Western blot analysis showed no significant correlation between them (Fig. 6B,C). ASO-Tri-GalNAc treatment resulted in the selective knockdown of hepatic *Fads1* without altering FADS2 mRNA expression (Fig. 6D,E), showing that ASO-Tri-GalNAc had a specific effect and did not affect the expression of *Fads2*. In addition, selective knockdown of hepatic *Fads1* did not significantly affect the weight of liver or white fat (epididymal fat) (Fig. 6F,G).

5. Discussion

Multiple factors cause atherosclerosis, indicating its complex pathogenesis, which has not been fully elucidated. Given that *Fads1* encodes $\Delta 5$ fatty acid desaturase and that its metabolites play essential roles in the inflammatory response and atherosclerosis, the exploration of FADS1 has become a hot topic in recent years [25].

Powell *et al.* [12] showed that ApoE^{-/-} mice reduced body weight, improved glycemia, and reduced atherosclerotic plaques after *Fads1* knockout. This study showed that deletion of *Fads1* was associated with a reduced inflammatory response in the arterial wall, mainly in the form of a lower arachidonic acid (ARA)/linoleic acid ratio in plasma and adipose tissue, which positively affected the prevention of atherosclerosis. Takagahara *et al.* [14] found that an orally available FADS1 inhibitor prevented atherosclerosis accompanied by changes in fatty acid composition and eicosanoid production in ApoE^{-/-} mice. Gromovsky *et al.* [13] used ASOs to specifically knockdown *Fads1* in the liver, adipose, and reticuloendothelial system of LDL receptor null (LDLR^{-/-}) mice, which resulted in exacer-

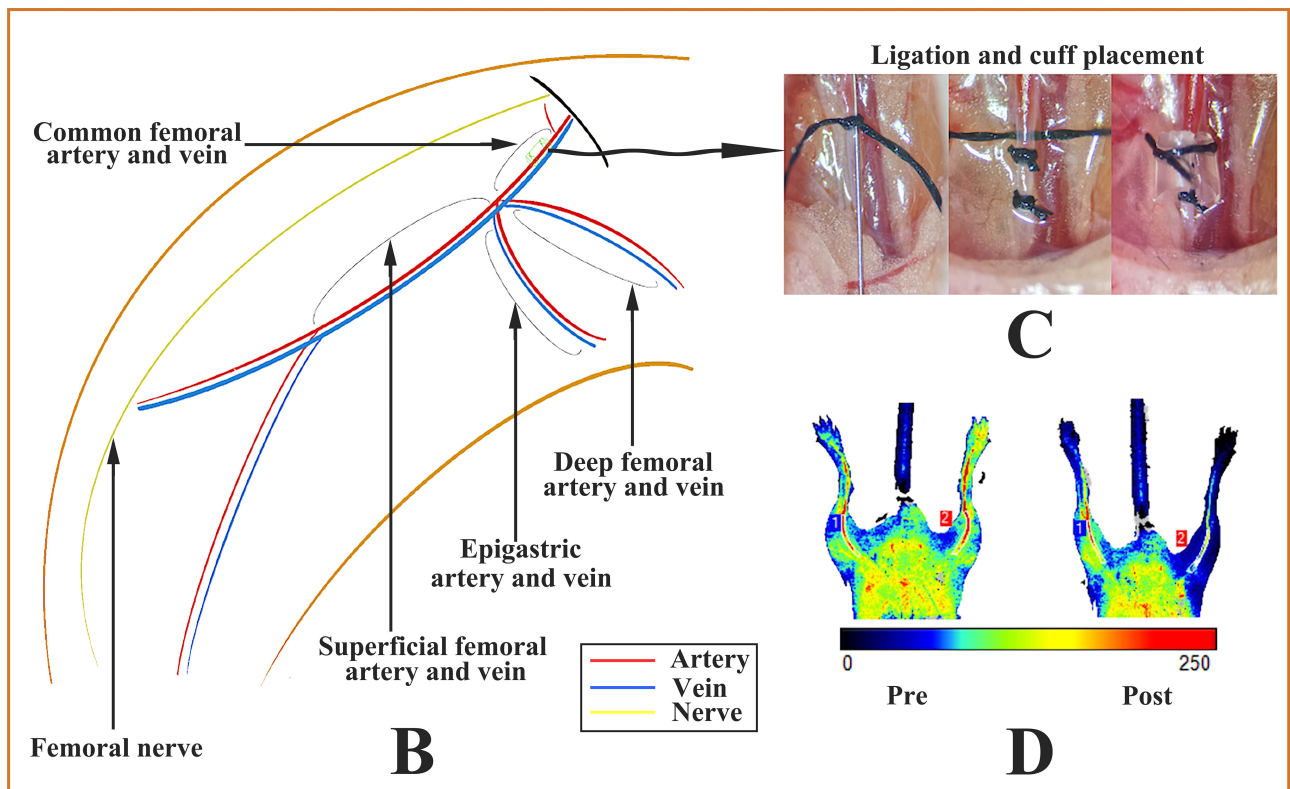
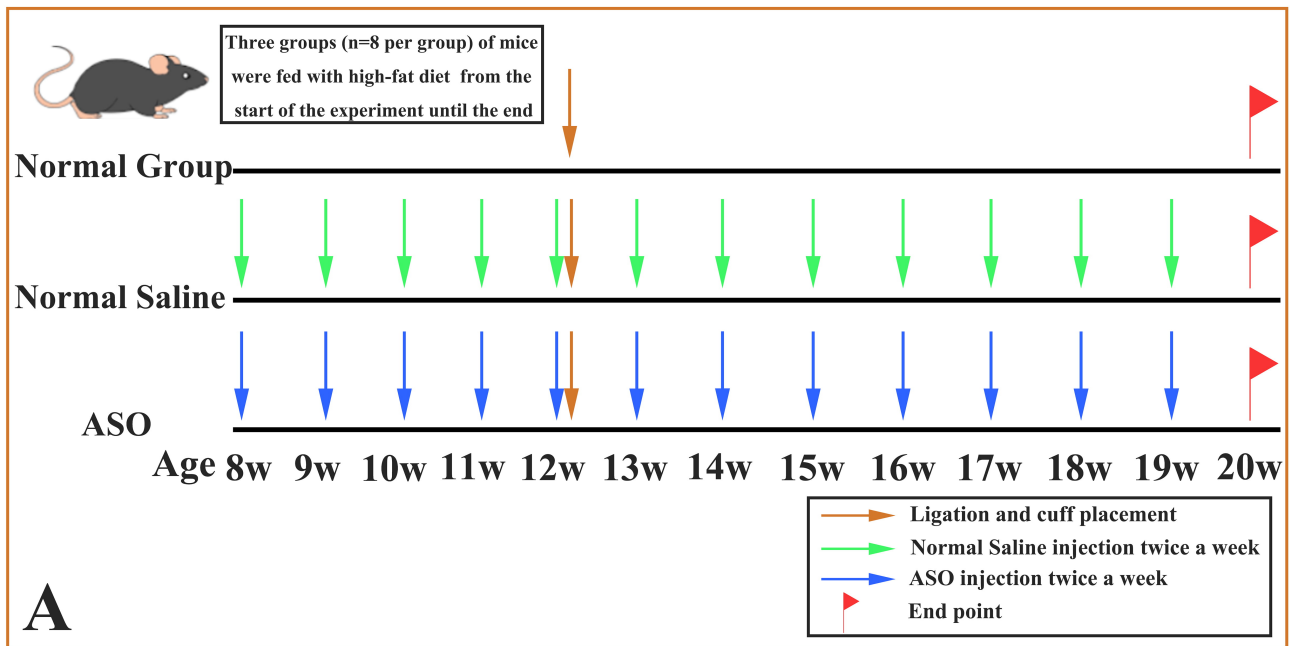


Fig. 2. Different interventions in the three groups of mice and modeling process of atherosclerosis in mouse femoral arteries. (A) During the experimental cycle, the three groups of mice were subjected to different interventions. (B) Vascular anatomy of the mouse right lower limb. (C) Right femoral artery cuff placement combined with tandem stenosis. (D) Preoperative (left) and postoperative (right) laser Doppler perfusion imaging of mice showed postoperative stenosis of the right femoral artery and decreased perfusion of the distal femoral artery.

bated atherosclerosis and liver inflammation. These results were different from the previous two studies, but were in agreement with the results of this study. Given these dis-

crepant results, Gromovsky *et al.* [13] speculated that the model in the study by Powell *et al.* [12] produced a hypomorphic allele rather than a complete loss function allele,

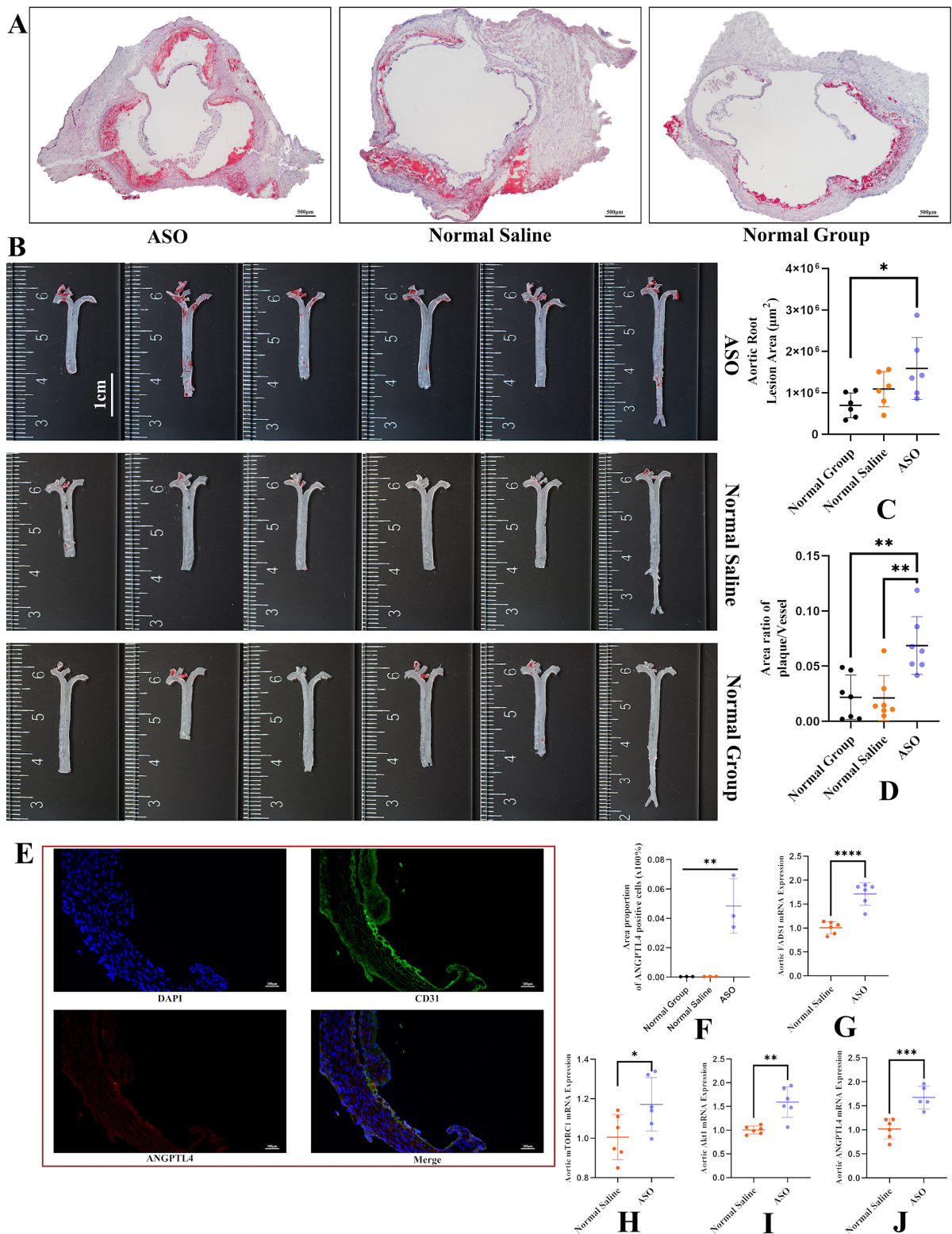


Fig. 3. Quantitative analysis of aortic plaque and upregulated expression of angiopoietin-like 4 (ANGPTL4) in the aorta with more severe atherosclerosis. (A) Representative Oil Red O staining of aortic roots in the three groups. Scale bar, 500 μm . (B) Aortic Oil Red O staining in the three groups. Scale bar, 1 cm. (C) Quantitative analysis of aortic root plaque area ($n = 6$). (D) Quantitative analysis of the ratio of plaque area to aortic area ($n = 6$). (E) Representative images of aortic root from mice treated with *Fads1*-ASO. Sections were immunostained with CD31, in green. Sections were immunostained with ANGPTL4, in red. Scale bar, 100 μm . (F) Quantitative analysis of the area proportion of ANGPTL4-positive cells ($n = 3$). (G–J) *FADS1*, *mTOCR1*, *AKT1*, and *ANGPTL4* mRNA expression in the aorta (abdominal aorta to iliac artery); $n = 6$ per group. *, $p < 0.05$, **, $p < 0.01$, ***, $p < 0.001$, ****, $p < 0.0001$.

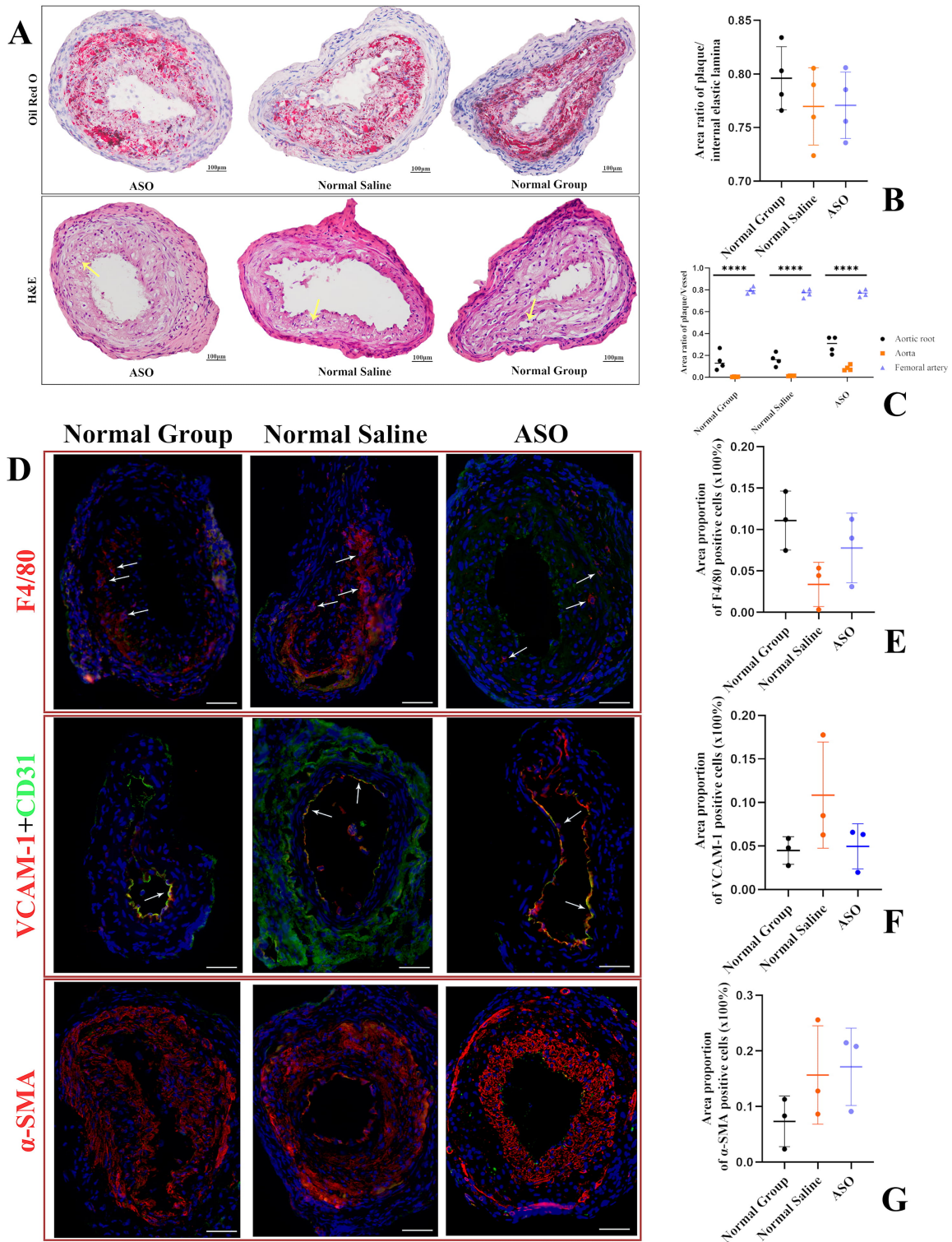


Fig. 4. Quantitative analysis of femoral artery plaque and representative images of femoral artery from three groups. (A) Vessels between the ligation sites of the two ends of the femoral artery were stained with Oil Red O and H&E. Oil Red O staining showed atherosclerotic plaque formation and a larger lipid core in all three groups. Hematoxylin-Eosin staining H&E staining showed disturbed endothelial cell arrangement and foam cell aggregation. The arrow in the figure shows typical foam cells. Scale bar, 100 μ m. (B) The ratio of plaque area to the area under the internal elastic plate (n = 4). (C) The ratio of plaque area to the vessel or area under the internal elastic plate (n = 4). (D) Sections were immunostained with F4/80, VCAM-1, and α -SMA, in red. Sections were immunostained with CD31, in green. The arrow in the figure shows typical cells. Scale bar, 100 μ m. (E–G) Area proportion of F4/80, VCAM-1, and α -SMA-positive cells (n = 3). ****, $p < 0.0001$.

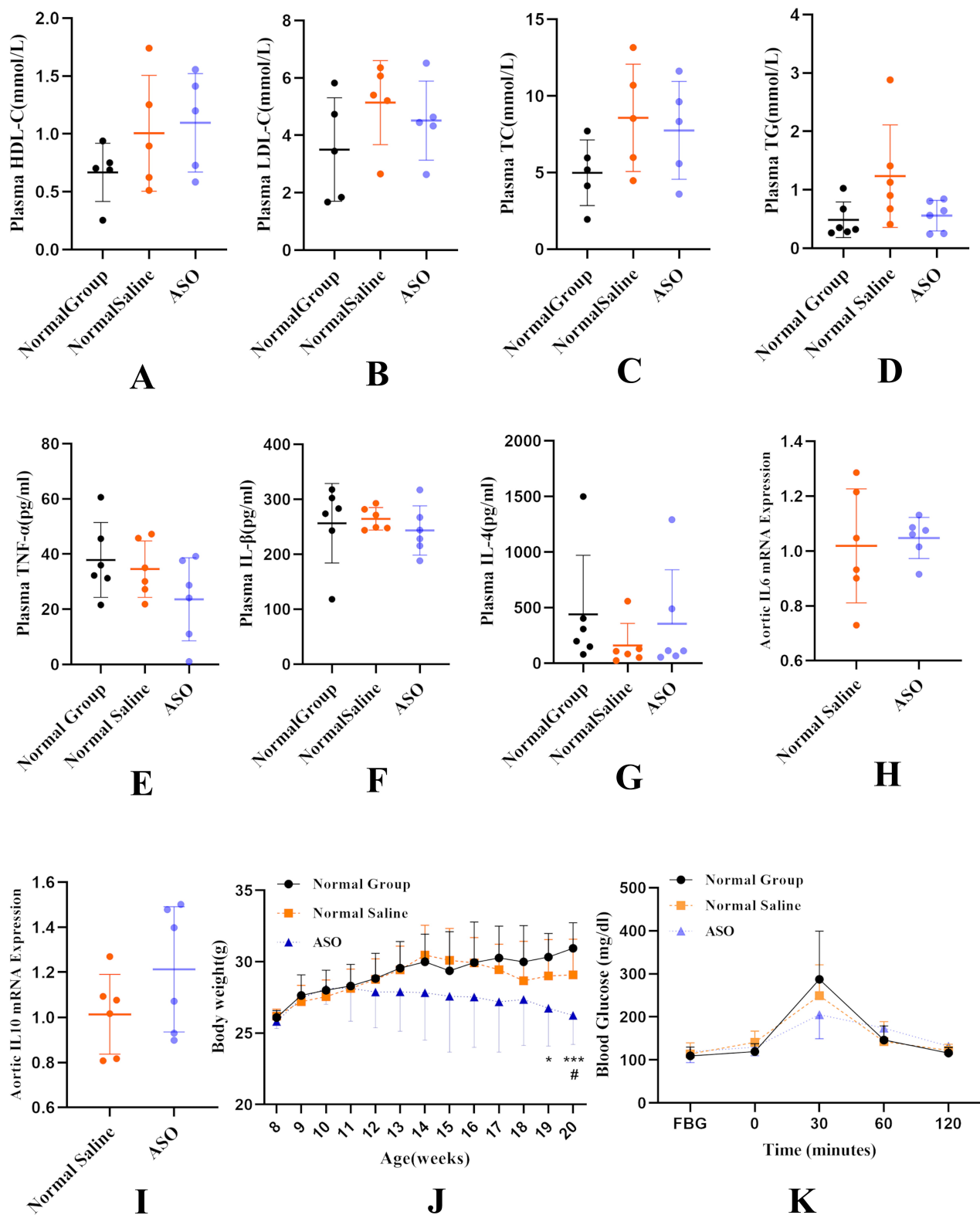


Fig. 5. Knockdown of liver *Fads1* aggravated atherosclerosis without significantly changing plasma lipid and inflammatory cytokine levels, reduced body weight, and improved glycemic control. (A,B) High-density lipoprotein cholesterol (HDL-C), and low-density lipoprotein cholesterol (LDL-C) levels after 12 weeks of high-fat diet in the three groups; n = 6 per group. (C,D) Plasma total cholesterol and total triglyceride; n = 6 per group. (E–G) Plasma tumor necrosis factor α , IL- β , and IL-4 levels; n = 6 per group. (H,I) IL-6 and IL-10 mRNA expression in the aorta (abdominal aorta to iliac artery); n = 6 per group. (J) Body weight curves over the study period; n = 8 per group. (K) Glucose tolerance tests of three groups; n = 7 per group. *, $p < 0.05$, ***, $p < 0.001$, #, $p < 0.05$.

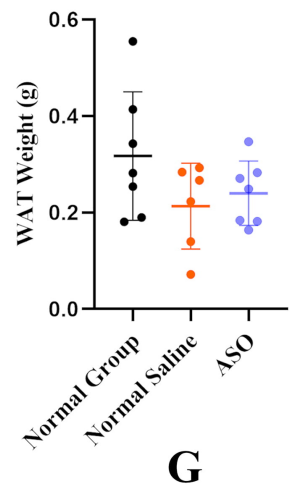
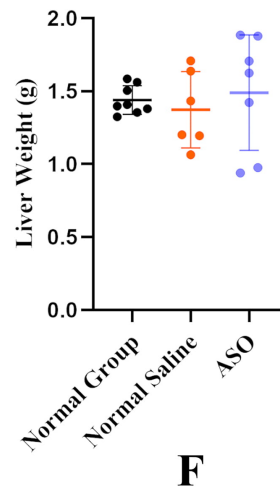
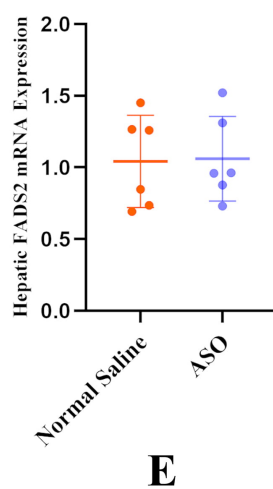
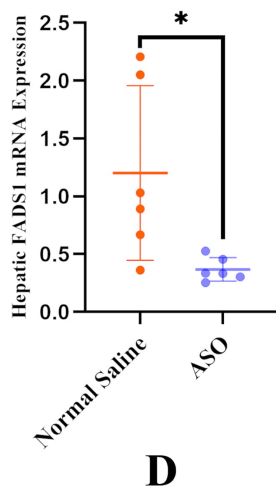
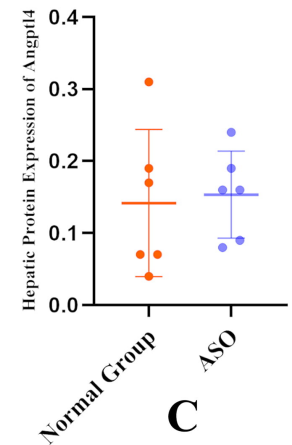
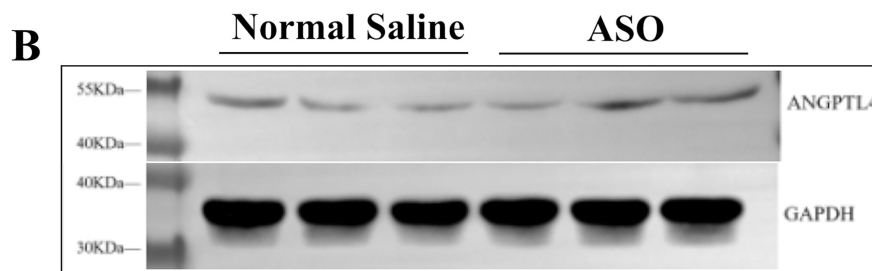
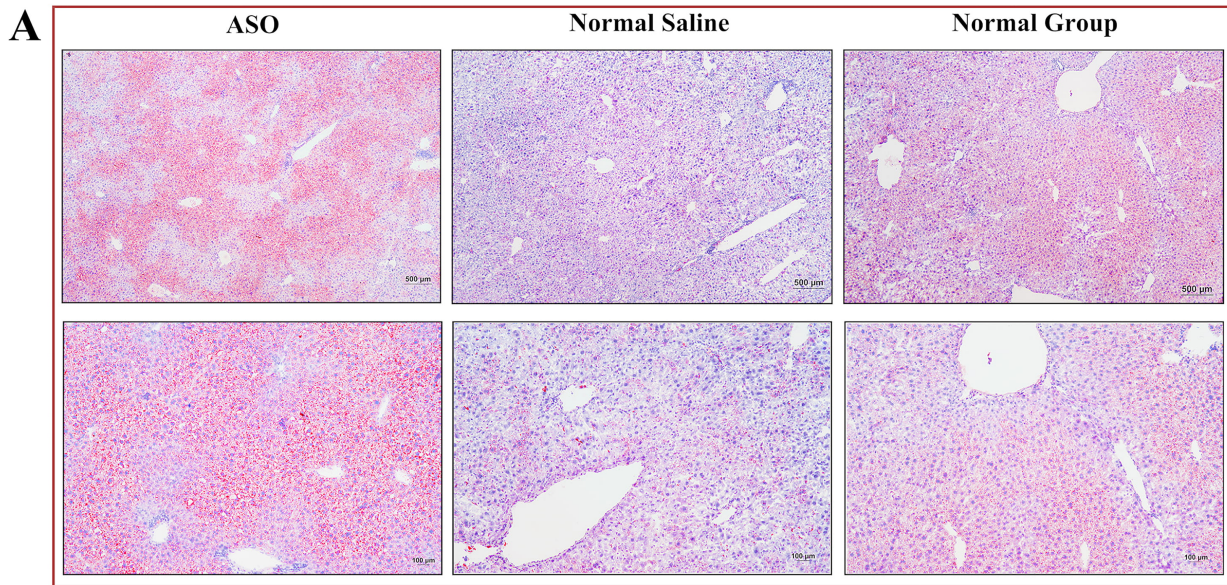


Fig. 6. Knockdown of liver *Fads1* aggravated non-alcoholic fatty liver disease (NAFLD). (A) Representative images of liver Oil Red O staining in three groups. View at 40 \times (above), scale bar, 500 μ m. View at 100 \times (below), scale bar, 100 μ m. (B) Western blot analysis of ANGPTL4 expression in liver from the Normal Saline Group and ASO Group (n = 6, per group); GAPDH was used as a loading control. (C) Quantitative analysis of ANGPTL4 expression in the liver. (D,E) FADS1 and FADS2 mRNA expression in the liver (n = 6). (F,G) Liver and white adipose tissue weight of the three groups (n = 7). *, $p < 0.05$.

and the hepatic expression levels of FADS1 were not reported. Although the genetic background of the mice in our study differed from that used in Gromovsky's study, our study suggested that the downregulation of hepatic FADS1 expression exacerbates atherosclerosis and NAFLD, probably because *Fads1* knockdown is associated with chronic inflammation caused by its regulated metabolites such as eicosapentaenoic acid (EPA) and arachidonic acid (ARA). In addition, previous studies have reported similar improvements in body weight and glucose tolerance with *Fads1* loss of function mice in the ApoE^{-/-} and LDLR^{-/-} background [12,13]. Although knockdown of hepatic *Fads1* could aggravate NAFLD, it had no significant effect on the weight of liver and white fat (epididymal fat). The worsening of NAFLD due to hepatic *Fads1* knockdown is incredibly likely associated with the reorganization of lipid metabolism gene expression. Gromovsky *et al.* [13] showed that *Fads1* knockdown significantly reduced the expression of the master lipogenic transcription factors Srebp1c (sterol regulatory element binding proteins 1c) and 2 (Srebp2) and their downstream target genes, including *Acc1* (acetyl-CoA carboxylase 1), and fatty acid synthase in the liver, which leads to the accumulation of lipids in the liver. In addition, weight loss due to hepatic *Fads1* knockdown may be associated with enhanced auto metabolism, as this is consistent with the results of improved glucose tolerance. In the future, exploring whether *Fads1* knockdown affects oxygen consumption, carbon dioxide production, and respiratory exchange rate could further elucidate the cause of weight loss. It is worth noting that the use of Tri-GalNAc-ASOs significantly inhibited the expression of *Fads1* in liver cells only, whereas *Fads1* was expressed in all tissues, and variants of *Fads1* may also produce different phenotypes. In the future, a non-ASO approach to explore each *Fads1* single nucleotide polymorphism (SNP) individual is required to understand the genetic associations behind the disease entirely.

After *Fads1* knockdown in the liver of ApoE^{-/-} mice, the plasma lipids and inflammatory factors levels did not change significantly, indicating that the circulating proatherogenic factors did not play a significant role in this study. The aortic root lesion area in the Normal Saline Group did not statistically differ from the ASO Group; aortic root staining may appear different depending on the location of the section, which is unreliable. Therefore, aortic Oil Red O staining can more effectively reflect the situation of atherosclerosis among the three groups. Since it is challenging to form atherosclerosis spontaneously in peripheral vessels (i.e., femoral artery) in mice, to accelerate the formation of femoral artery atherosclerosis, we established the model to explore the effects of hepatic *Fads1* knockdown on peripheral blood vessels. All three groups of mice showed macrophage infiltration and smooth muscle cell hyperplasia at the site of femoral artery atherosclerosis; meanwhile, the expression of VCAM-1, a leukocyte adhesion-

promoting and inflammation-promoting molecule, was also elevated. These results suggest that placement of a perivascular cuff combined with tandem stenosis can successfully induce atherosclerotic lesions in the femoral arteries, which is associated with a pro-inflammatory response mediated by upregulation of VCAM-1 expression. Another finding was that hepatic *Fads1* knockdown did not aggravate surgically induced lower limb atherosclerosis. Although there was no difference in the degree of atherosclerosis of the femoral artery among the three groups of mice, there was a significant difference compared with their own spontaneous atherosclerosis. We considered that altered hemodynamics and shear stress are responsible for the exacerbation of femoral atherosclerosis, not the downregulation of hepatic FADS1 expression. In other words, the difference in the degree of aortic and peripheral atherosclerosis is mainly manifested by whether inhibition of liver *Fads1* is more dominant or changes in hemodynamics and shear stress are more dominant. The results showed that surgical intervention may interfere with the effect of reduced liver FADS1 expression on femoral atherosclerosis compared with aortic atherosclerosis; selective ASO-mediated knockdown of liver *Fads1* significantly aggravated spontaneous aortic atherosclerosis but did not affect femoral atherosclerosis caused by surgical intervention.

Endothelial cells are the main component of the endothelial barrier, and destruction of the endothelial barrier leads to changes in vascular permeability. Endothelial dysfunction is responsible for the initiation of atherosclerosis, which contributes to the occurrence of atherosclerosis [26,27]. Although the effect of ANGPTL4 on atherosclerosis remains a subject of debate [28–30], multiple studies have shown that ANGPTL4 promotes vascular inflammation and increases vascular permeability [31–37]. Adipose tissue and liver-derived ANGPTL4 might promote atherogenesis by regulating lipid uptake and inflammation in other tissues [38–40]. Furthermore, ANGPTL4 might promote atherogenesis through its vascular effects independently of the regulation of circulating lipids. ANGPTL4 mediates the inhibition of lipoprotein lipase (LPL) activity under different circumstances, and accumulating evidence has shown a direct correlation between ANGPTL4 and the risk of atherosclerosis. Although ANGPTL4 is a secreted protein, ANGPTL4 also controls lipoprotein metabolism and energy homeostasis as well as LPL-independent functions in the tissues where it is expressed, the relative contributions of cell-intrinsic and endothelial-specific versus circulating ANGPTL4 from other sources in regulating these processes are unclear [38]. Li *et al.* [41] indicated that FADS1 could activate AKT/mTOR signaling, and this hypothesis was further validated by both *in vivo* and *in vitro* assays. In addition, RNA sequencing revealed ANGPTL4 as a candidate downstream gene of the mTOR pathway [42]. In light of these conclusions, we speculated that FADS1 could affect atheroscle-

rosis through AKT/mTOR signaling. In this study, we quantitatively analyzed the expression of ANGPTL4 in arterial endothelial cells, aorta, and liver. We found that ANGPTL4 expression was upregulated in the mouse aorta with more severe atherosclerosis, consistent with the upregulated mRNA expression of FADS1 and AKT1/mTORC1 (Fig. 3E–J). Furthermore, we inhibited hepatic FADS1 mRNA expression; however, the expression of ANGPTL4 was not affected (Fig. 6B–D), which may be related to the expression of ANGPTL4 in the liver being also regulated by nutritional and metabolic states [38]. The above results suggest that liver-derived ANGPTL4 is not responsible for the exacerbation of atherosclerosis, but the arterial endothelium-derived ANGPTL4 may exacerbate atherosclerosis. Therefore, we speculated that the upregulation of FADS1 expression could exacerbate atherosclerosis by upregulating ANGPTL4 expression in the aorta through AKT1/mTORC1 signaling. However, this study had some limitations. We did not analyze the expression of AKT1/phospho-AKT1 or mTORC1/phospho-mTORC1 by Western blotting. In the future, further validation of whether FADS1 in arterial endothelial cells can affect ANGPTL4 expression via the mTORC1/AKT1 signaling pathway and whether it further affects LPL activity is required.

Interestingly, the mRNA expression of FADS1 in the liver and vessel was inconsistent. ASO inhibited hepatic FADS1 mRNA expression, but FADS1 mRNA expression was upregulated in the aorta. We suggest that the upregulation of FADS1 mRNA expression in the vessel was not significantly associated with ASO: (1) ASO underwent Tri-GalNAc modification by targeting hepatocytes and is unlikely to have the ability to bind to vascular tissues; (2) the metabolic sites and accumulation sites of ASO, even without modification, are mainly concentrated in the liver, adipose, kidney, and reticuloendothelial cell systems, lacking selectivity for vascular tissues; and (3) ASO inhibits the expression rather than promotes the expression of target genes. We speculated that selective knockdown of hepatic FADS1, a key enzyme in the metabolism of ω -3 and ω -6 PUFAs, resulted in diminished levels of ARA, EPA, and docosahexaenoic acid (DHA)- derived proinflammatory and pro-resolving lipid mediators and reduced secretion to tissues and organs [13], vascular endothelial cells have compensatory upregulation of FADS1 expression due to reduced intake of these lipid mediators and this leads to inconsistent expression of FADS1 in liver and vascular endothelial cells. In summary, this study demonstrated that ASO-Tri-GalNAc-mediated knockdown of hepatic *Fads1* exacerbated atherosclerosis; FADS1 expression was upregulated in aorta with more severe atherosclerosis and was accompanied by upregulation of ANGPTL4 expression, in which AKT1/mTORC1 pathway may be involved. This study provides a new perspective to explore the effect of FADS1 on atherosclerosis.

6. Conclusions

In the current study, we demonstrated that knockdown of liver *Fads1* aggravated aortic atherosclerosis without significantly changing plasma LDL-C, HDL-C secretion rates, and inflammatory cytokine levels. We also found that ANGPTL4 expression was upregulated in the mouse aorta with more severe atherosclerosis, consistent with the upregulated mRNA expression of FADS1 and AKT1/mTORC1. Interestingly, selective knockdown of liver *Fads1* had no significant effect on femoral atherosclerosis caused by surgical intervention. ASO-Tri-GalNAc-treated mice exhibited more severe NAFLD. In addition, knockdown of liver *Fads1* reduced body weight and improved glycemic control. We also emphasize the need for an in-depth exploration of the regulation of FADS1-AKT1/mTORC1-ANGPTL4-LPL signaling in arterial endothelial cells for atherosclerosis to more clearly elucidate the molecular mechanism underlying FADS1 regulation of atherosclerosis.

Availability of Data and Materials

The primer sequence is available in the supplementary material. The datasets used or analyzed during the current study are available from the corresponding author on reasonable request.

Author Contributions

QL, PW and SW planned the project; QL designed diets, designed experiments, analyzed data, and wrote the article; QL, ZY, YD conducted mouse experiments, performed biochemical workup of mouse tissues, and aided in article preparation; all authors were involved in the editing of the final article. All authors read and approved the final manuscript. All authors have participated sufficiently in the work and agreed to be accountable for all aspects of the work.

Ethics Approval and Consent to Participate

All mouse experiments were performed according to the local relevant guidelines. All mice were kept under specific pathogen-free conditions in the Beijing Institute of Heart Lung and Blood Vessel Diseases and given free access to food and water. Our study was approved by the Ethics Committee of Beijing Anzhen Hospital (ethics number: 2022174X). The investigation conformed to the Guide for the Care and Use of Laboratory Animals published by the US National Institutes of Health (NIH Publication No. 85-23, 1996, revised 2011; available from www.nap.edu/catalog/5140.html).

Acknowledgment

Not applicable.

Funding

This study was supported by grants from the Director's Fund of Beijing Anzhen Hospital (2022409422 to S.W.).

Conflict of Interest

The authors declare no conflict of interest.

Supplementary Material

Supplementary material associated with this article can be found, in the online version, at <https://doi.org/10.31083/j.fbl2904131>.

References

- [1] Tsurutani Y, Inoue K, Sugisawa C, Saito J, Omura M, Nishikawa T. Increased Serum Dihomo- γ -linolenic Acid Levels Are Associated with Obesity, Body Fat Accumulation, and Insulin Resistance in Japanese Patients with Type 2 Diabetes. *Internal Medicine (Tokyo, Japan)*. 2018; 57: 2929–2935.
- [2] Kwong RY, Heydari B, Ge Y, Abdullah S, Fujikura K, Kaneko K, *et al.* Genetic profiling of fatty acid desaturase polymorphisms identifies patients who may benefit from high-dose omega-3 fatty acids in cardiac remodeling after acute myocardial infarction-Post-hoc analysis from the OMEGA-REMODEL randomized controlled trial. *PLoS One*. 2019; 14: e0222061.
- [3] Koletzko B, Reischl E, Tanjung C, Gonzalez-Casanova I, Ramakrishnan U, Meldrum S, *et al.* *FADS1* and *FADS2* Polymorphisms Modulate Fatty Acid Metabolism and Dietary Impact on Health. *Annual Review of Nutrition*. 2019; 39: 21–44.
- [4] Chen J, Ruan X, Sun Y, Li X, Yuan S, Larsson SC. Plasma phospholipid arachidonic acid in relation to non-alcoholic fatty liver disease: Mendelian randomization study. *Nutrition (Burbank, Los Angeles County, Calif.)*. 2023; 106: 111910.
- [5] Huang PC, Cheng H, Su YT, Huang MC, Hsu CC, Hwang SJ, *et al.* Interaction among dietary n-3 and n-6 polyunsaturated fatty acid intake, fatty acid desaturase 2 genetic variants, and low-density lipoprotein cholesterol levels in type 2 diabetes patients. *Journal of Diabetes Investigation*. 2023; 14: 297–308.
- [6] O'Neill CM, Minihane AM. The impact of fatty acid desaturase genotype on fatty acid status and cardiovascular health in adults. *The Proceedings of the Nutrition Society*. 2017; 76: 64–75.
- [7] Juan J, Huang H, Jiang X, Ardisson Korat AV, Song M, Sun Q, *et al.* Joint effects of fatty acid desaturase 1 polymorphisms and dietary polyunsaturated fatty acid intake on circulating fatty acid proportions. *The American Journal of Clinical Nutrition*. 2018; 107: 826–833.
- [8] de Toro-Martín J, Guénard F, Rudkowska I, Lemieux S, Couture P, Vohl MC. A common variant in ARHGEF10 alters delta-6 desaturase activity and influence susceptibility to hypertriglyceridemia. *Journal of Clinical Lipidology*. 2018; 12: 311–320.e3.
- [9] Marklund M, Morris AP, Mahajan A, Ingelsson E, Lindgren CM, Lind L, *et al.* Genome-Wide Association Studies of Estimated Fatty Acid Desaturase Activity in Serum and Adipose Tissue in Elderly Individuals: Associations with Insulin Sensitivity. *Nutrients*. 2018; 10: 1791.
- [10] Yuan S, Bäck M, Bruzelius M, Mason AM, Burgess S, Larsson S. Plasma Phospholipid Fatty Acids, *FADS1* and Risk of 15 Cardiovascular Diseases: A Mendelian Randomisation Study. *Nutrients*. 2019; 11: 3001.
- [11] Chen HY, Cairns BJ, Small AM, Burr HA, Ambikumar A, Martinsson A, *et al.* Association of *FADS1/2* Locus Variants and Polyunsaturated Fatty Acids With Aortic Stenosis. *JAMA Cardiology*. 2020; 5: 694–702.
- [12] Powell DR, Gay JP, Smith M, Wilganowski N, Harris A, Holland A, *et al.* Fatty acid desaturase 1 knockout mice are lean with improved glycemic control and decreased development of atherosclerotic plaque. *Diabetes, Metabolic Syndrome and Obesity: Targets and Therapy*. 2016; 9: 185–199.
- [13] Gromovsky AD, Schugar RC, Brown AL, Helsley RN, Burrows AC, Ferguson D, *et al.* Δ -5 Fatty Acid Desaturase *FADS1* Impacts Metabolic Disease by Balancing Proinflammatory and Proresolving Lipid Mediators. *Arteriosclerosis, Thrombosis, and Vascular Biology*. 2018; 38: 218–231.
- [14] Takagahara S, Shinohara H, Itokawa S, Satomi Y, Ando A, Yamamoto T, *et al.* A Novel Orally Available Delta-5 Desaturase Inhibitor Prevents Atherosclerotic Lesions Accompanied by Changes in Fatty Acid Composition and Eicosanoid Production in *ApoE* Knockout Mice. *The Journal of Pharmacology and Experimental Therapeutics*. 2019; 371: 290–298.
- [15] Guo FX, Wu Q, Li P, Zheng L, Ye S, Dai XY, *et al.* The role of the lncRNA-FA2H-2-MLKL pathway in atherosclerosis by regulation of autophagy flux and inflammation through mTOR-dependent signaling. *Cell Death and Differentiation*. 2019; 26: 1670–1687.
- [16] Fan YY, Monk JM, Hou TY, Callway E, Vincent L, Weeks B, *et al.* Characterization of an arachidonic acid-deficient (*Fads1* knockout) mouse model. *Journal of Lipid Research*. 2012; 53: 1287–1295.
- [17] Fan YY, Callaway E, Monk J, Goldsby J, Yang P, Vincent L, *et al.* A New Model to Study the Role of Arachidonic Acid in Colon Cancer Pathophysiology. *Cancer Prevention Research (Philadelphia, Pa.)*. 2016; 9: 750–757.
- [18] Cabral F, Miller CM, Kudrna KM, Hass BE, Daubendiek JG, Kellar BM, *et al.* Purification of Hepatocytes and Sinusoidal Endothelial Cells from Mouse Liver Perfusion. *Journal of Visualized Experiments: JoVE*. 2018; 56993.
- [19] Moroi M, Zhang L, Yasuda T, Virmani R, Gold HK, Fishman MC, *et al.* Interaction of genetic deficiency of endothelial nitric oxide, gender, and pregnancy in vascular response to injury in mice. *The Journal of Clinical Investigation*. 1998; 101: 1225–1232.
- [20] von der Thüsen JH, van Berkel TJ, Biessen EA. Induction of rapid atherogenesis by perivascular carotid collar placement in apolipoprotein E-deficient and low-density lipoprotein receptor-deficient mice. *Circulation*. 2001; 103: 1164–1170.
- [21] Stoffel W, Binczek E, Schmidt-Soltau I, Brodessaer S, Wegner I. High fat / high cholesterol diet does not provoke atherosclerosis in the ω 3- and ω 6-polyunsaturated fatty acid synthesis-inactivated Δ 6-fatty acid desaturase-deficient mouse. *Molecular Metabolism*. 2021; 54: 101335.
- [22] Stoffel W, Schmidt-Soltau I, Binczek E, Thomas A, Thevis M, Wegner I. Dietary ω 3- and ω 6-Polyunsaturated fatty acids reconstitute fertility of Juvenile and adult *Fads2*-Deficient mice. *Molecular Metabolism*. 2020; 36: 100974.
- [23] Jensen EC. Quantitative analysis of histological staining and fluorescence using ImageJ. *Anatomical Record (Hoboken, N.J.)*. 2007; 296: 378–381.
- [24] Revelli JP, Smith D, Allen J, Jeter-Jones S, Shadoan MK, Desai U, *et al.* Profound obesity secondary to hyperphagia in mice lacking kinase suppressor of ras 2. *Obesity (Silver Spring, Md.)*. 2011; 19: 1010–1018.
- [25] Panda C, Varadaraj S, Voruganti VS. PUFA, genotypes and risk for cardiovascular disease. *Prostaglandins, Leukotrienes, and Essential Fatty Acids*. 2022; 176: 102377.
- [26] Davignon J, Ganz P. Role of endothelial dysfunction in atherosclerosis. *Circulation*. 2004; 109: III27–III32.
- [27] Chiu JJ, Chien S. Effects of disturbed flow on vascular endothelium: pathophysiological basis and clinical perspectives. *Physiological Reviews*. 2011; 91: 327–387.
- [28] Aryal B, Rotllan N, Araldi E, Ramirez CM, He S, Chouster-

- man BG, *et al.* ANGPTL4 deficiency in haematopoietic cells promotes monocyte expansion and atherosclerosis progression. *Nature Communications*. 2016; 7: 12313.
- [29] Dewey FE, Gusarova V, O'Dushlaine C, Gottesman O, Trejos J, Hunt C, *et al.* Inactivating Variants in ANGPTL4 and Risk of Coronary Artery Disease. *The New England Journal of Medicine*. 2016; 374: 1123–1133.
- [30] Lichtenstein L, Mattijssen F, de Wit NJ, Georgiadi A, Hooiveld GJ, van der Meer R, *et al.* Angptl4 protects against severe proinflammatory effects of saturated fat by inhibiting fatty acid uptake into mesenteric lymph node macrophages. *Cell Metabolism*. 2010; 12: 580–592.
- [31] Ehrlich KC, Lacey M, Ehrlich M. Tissue-specific epigenetics of atherosclerosis-related ANGPT and ANGPTL genes. *Epigenomics*. 2019; 11: 169–186.
- [32] Serbanovic-Canic J, de Luca A, Warboys C, Ferreira PF, Luong LA, Hsiao S, *et al.* Zebrafish Model for Functional Screening of Flow-Responsive Genes. *Arteriosclerosis, Thrombosis, and Vascular Biology*. 2017; 37: 130–143.
- [33] Theofilatos D, Fotakis P, Valanti E, Sanoudou D, Zannis V, Kardassis D. HDL-apoA-I induces the expression of angiopoietin like 4 (ANGPTL4) in endothelial cells via a PI3K/AKT/FOXO1 signaling pathway. *Metabolism: Clinical and Experimental*. 2018; 87: 36–47.
- [34] Chong HC, Chan JSK, Goh CQ, Gounko NV, Luo B, Wang X, *et al.* Angiopoietin-like 4 stimulates STAT3-mediated iNOS expression and enhances angiogenesis to accelerate wound healing in diabetic mice. *Molecular Therapy: the Journal of the American Society of Gene Therapy*. 2014; 22: 1593–1604.
- [35] Li H, Ge C, Zhao F, Yan M, Hu C, Jia D, *et al.* Hypoxia-inducible factor 1 alpha-activated angiopoietin-like protein 4 contributes to tumor metastasis via vascular cell adhesion molecule-1/integrin β 1 signaling in human hepatocellular carcinoma. *Hepatology (Baltimore, Md.)*. 2011; 54: 910–919.
- [36] Huang RL, Teo Z, Chong HC, Zhu P, Tan MJ, Tan CK, *et al.* ANGPTL4 modulates vascular junction integrity by integrin signaling and disruption of intercellular VE-cadherin and claudin-5 clusters. *Blood*. 2011; 118: 3990–4002.
- [37] Galaup A, Cazes A, Le Jan S, Philippe J, Connault E, Le Coz E, *et al.* Angiopoietin-like 4 prevents metastasis through inhibition of vascular permeability and tumor cell motility and invasiveness. *Proceedings of the National Academy of Sciences of the United States of America*. 2006; 103: 18721–18726.
- [38] Aryal B, Price NL, Suarez Y, Fernández-Hernando C. ANGPTL4 in Metabolic and Cardiovascular Disease. *Trends in Molecular Medicine*. 2019; 25: 723–734.
- [39] Aryal B, Singh AK, Zhang X, Varela L, Rotllan N, Goedeke L, *et al.* Absence of ANGPTL4 in adipose tissue improves glucose tolerance and attenuates atherogenesis. *JCI Insight*. 2018; 3: e97918.
- [40] Katanasaka Y, Saito A, Sunagawa Y, Sari N, Funamoto M, Shimizu S, *et al.* ANGPTL4 Expression Is Increased in Epicardial Adipose Tissue of Patients with Coronary Artery Disease. *Journal of Clinical Medicine*. 2022; 11: 2449.
- [41] Liu YZ, Zhang C, Jiang JF, Cheng ZB, Zhou ZY, Tang MY, *et al.* Angiopoietin-like proteins in atherosclerosis. *Clinica Chimica Acta; International Journal of Clinical Chemistry*. 2021; 521: 19–24.
- [42] Saito M, Mitani A, Ishimori T, Miyashita N, Isago H, Mikami Y, *et al.* Active mTOR in Lung Epithelium Promotes Epithelial-Mesenchymal Transition and Enhances Lung Fibrosis. *American Journal of Respiratory Cell and Molecular Biology*. 2020; 62: 699–708.